Optical properties of a periodic monolayer of metallic nanospheres on a dielectric waveguide

2005 J. Phys.: Condens. Matter 17 1791

(http://iopscience.iop.org/0953-8984/17/12/003)

INSTITUTE OF PHYSICS PUBLISHING JOURNAL OF PHYSICS: CONDENSED MATTER

J. Phys.: Condens. Matter **17** (2005) 1791–1802 doi:10.1088/0953-8984/17/12/003

Optical properties of a periodic monolayer of metallic nanospheres on a dielectric waveguide

G Gantzounis[1,3], N Stefanou[1] and V Yannopapas[2]

[1] Section of Solid State Physics, University of Athens, Panepistimioupolis, GR-157 84 Athens, Greece
[2] School of Natural Sciences, Department of Materials Science, University of Patras, GR-265 04 Patras, Greece

E-mail: ggantzou@cc.uoa.gr

Received 20 December 2004, in final form 15 February 2005
Published 11 March 2005
Online at stacks.iop.org/JPhysCM/17/1791

Abstract

The optical properties of a dielectric waveguide coated on one side with a periodic monolayer of metallic nanospheres are studied by means of transmission and density-of-states calculations using the on-shell layer-multiple-scattering method. In particular, the strong coupling mechanism between the waveguide and collective particle–plasmon modes is analysed and its influence on the optical response of the system is elucidated.

1. Introduction

Periodic structuring on a length scale comparable to the wavelength of light offers impressive possibilities in the exploitation of light–matter interaction. Recent advances in electron-beam lithography and self-assembly nanofabrication techniques allow one to prepare well-defined systems of nanoparticles with a tailored shape, size and arrangement, and observe new, interesting and potentially useful physical phenomena [1–5]. Among these systems, of particular interest are photonic crystal slabs consisting of a two-dimensional (2D) periodic array of metallic nanoparticles on a high-refractive-index dielectric guiding film. These systems exhibit guided resonances which are strongly confined within the slab and significantly affect the transmission of externally incident light. The above resonances originate from the interaction between guided eigenmodes of the dielectric film and collective particle–plasmon modes of the array of nanoparticles which leads to drastic modifications of the optical response of the nanoparticles with respect to the single-particle case [3, 6]. Similar effects have also been observed in structures with one-dimensional (1D) periodicity (metallic nanowire arrays on top of a dielectric waveguide), and have been analysed by means of numerical calculations using the

[3] Author to whom any correspondence should be addressed.

plane-wave scattering-matrix method [6–8]. This method is suitable for 1D structures and/or rectangular geometries [9]; however, for systems of nanoparticles it is not computationally efficient.

The purpose of the present paper is to present a thorough analysis of the resonance states of a 2D periodic array of noble-metal nanospheres on a dielectric waveguide, by means of first-principles calculations using the on-shell layer-multiple-scattering method [10–12]. This method applies equally well to non-absorbing systems and to absorbing ones (materials characterized by a complex dielectric function), and it can deal efficiently with systems containing strongly dispersive materials such as real metals. The frequency and radiative lifetime of the above resonance states are deduced directly from the corresponding spectral density of states of the electromagnetic (EM) field. Their symmetry and optical activity are analysed in conjunction with relevant transmission spectra, for normal incidence as well as for incidence at an angle. Our analysis elucidates the complex spectra associated with these resonances and provides a transparent picture of the underlying physical processes.

2. Surface–plasmon modes of a single metallic nanosphere

The electric field associated with a harmonic, monochromatic EM wave, of angular frequency ω, has the general form $\mathbf{E}(\mathbf{r},t) = \mathrm{Re}[\mathbf{E}(\mathbf{r})\exp(-\mathrm{i}\omega t)]$. For a plane wave of wavevector $\mathbf{q}$, propagating in a homogeneous medium characterized by a relative dielectric function ϵ and a relative magnetic permeability μ (we shall denote it by an index 0), $\mathbf{E}_0(\mathbf{r})$ can be expanded into regular vector spherical waves about a given origin of coordinates, as follows:

$$\mathbf{E}_0(\mathbf{r}) = \sum_{\ell=1}^{\infty}\sum_{m=-\ell}^{\ell}\left\{\frac{\mathrm{i}}{q}a^0_{E\ell m}\nabla\times j_\ell(qr)\mathbf{X}_{\ell m}(\hat{\mathbf{r}}) + a^0_{H\ell m}j_\ell(qr)\mathbf{X}_{\ell m}(\hat{\mathbf{r}})\right\}, \tag{1}$$

where $q = \omega\sqrt{\epsilon\mu}/c$, c being the velocity of light in vacuum; j_ℓ are the spherical Bessel functions which are finite everywhere; $\mathbf{X}_{\ell m}(\hat{\mathbf{r}})$ are the vector spherical harmonics; and $a^0_{E\ell m}$, $a^0_{H\ell m}$ are appropriate coefficients.

When the above field is incident on a given scatterer characterized by a different relative dielectric function ϵ_s and/or a different relative magnetic permeability μ_s, centred at the origin of coordinates, it produces a scattered field which, outside the scatterer, can be written as

$$\mathbf{E}_{\mathrm{sc}}(\mathbf{r}) = \sum_{\ell=1}^{\infty}\sum_{m=-\ell}^{\ell}\left\{\frac{\mathrm{i}}{q}a^+_{E\ell m}\nabla\times h^+_\ell(qr)\,\mathbf{X}_{\ell m}(\hat{\mathbf{r}}) + a^+_{H\ell m}h^+_\ell(qr)\,\mathbf{X}_{\ell m}(\hat{\mathbf{r}})\right\}, \tag{2}$$

where h^+_ℓ are the spherical Hankel functions appropriate to outgoing spherical waves: $h^+_\ell(qr) \simeq (-\mathrm{i})^\ell\exp(\mathrm{i}qr)/\mathrm{i}qr$ as $r\to\infty$. The coefficients in the above equation are determined from those of the incident field uniquely from the continuity of the EM field at the surface of the scatterer. In general we have

$$a^+_{P\ell m} = \sum_{P'=E,H}\sum_{\ell'=1}^{\infty}\sum_{m'=-\ell'}^{\ell'} T_{P\ell m;P'\ell'm'}a^0_{P'\ell'm'}. \tag{3}$$

In the following we shall consider the case of spherical scatterers for which we have $T_{P\ell m;P'\ell'm'} = T_{P\ell}\delta_{PP'}\delta_{\ell\ell'}\delta_{mm'}$, with

$$T_{E\ell}(\omega) = \left[\frac{j_\ell(q_\mathrm{s}r)\frac{\partial}{\partial r}[rj_\ell(qr)]\epsilon_\mathrm{s} - j_\ell(qr)\frac{\partial}{\partial r}[rj_\ell(q_\mathrm{s}r)]\epsilon}{h^+_\ell(qr)\frac{\partial}{\partial r}[rj_\ell(q_\mathrm{s}r)]\epsilon - j_\ell(q_\mathrm{s}r)\frac{\partial}{\partial r}[rh^+_\ell(qr)]\epsilon_\mathrm{s}}\right]_{r=S} \tag{4}$$

and

$$T_{H\ell}(\omega) = \left[\frac{j_\ell(q_s r)\frac{\partial}{\partial r}[r j_\ell(qr)]\mu_s - j_\ell(qr)\frac{\partial}{\partial r}[r j_\ell(q_s r)]\mu}{h_\ell^+(qr)\frac{\partial}{\partial r}[r j_\ell(q_s r)]\mu - j_\ell(q_s r)\frac{\partial}{\partial r}[r h_\ell^+(qr)]\mu_s} \right]_{r=S}, \tag{5}$$

where S is the radius of the sphere and $q_s = \omega\sqrt{\epsilon_s \mu_s}/c$.

With the help of the T matrix, defined above, one can calculate directly the change in the number of states up to a frequency ω between the system under consideration (a single scatterer in a host medium) and that of the host medium extending over all space:

$$\begin{aligned} \Delta N(\omega) &= \frac{1}{\pi} \operatorname{Im} \ln \det[\mathbf{I} + \mathbf{T}] \\ &= \frac{1}{\pi} \operatorname{Im} \sum_{\ell=1}^{\infty} (2\ell + 1) \ln[(1 + T_{E\ell})(1 + T_{H\ell})] \equiv \sum_{\ell=1}^{\infty} \Delta N_\ell(\omega), \end{aligned} \tag{6}$$

where $\mathbf{I}$ is the unit matrix [13, 14]. Of more interest is the difference in the density of states induced by the scatterer, given by $\Delta n(\omega) = \mathrm{d}\Delta N(\omega)/\mathrm{d}\omega$. The scattering cross section can be also expressed in terms of the T matrix as follows:

$$\sigma_{sc}(\omega) = \frac{\pi}{q^2} \sum_{\ell=1}^{\infty} (2\ell + 1)(|T_{E\ell}|^2 + |T_{H\ell}|^2). \tag{7}$$

Let us consider, to begin with, a single metallic sphere in air ($\epsilon = 1$, $\mu = 1$). We assume that the sphere is characterized by $\mu_s = 1$ and a Drude relative dielectric function [15]

$$\epsilon_s(\omega) = 1 - \frac{\omega_p^2}{\omega(\omega + \mathrm{i}\tau^{-1})}, \tag{8}$$

where ω_p is the bulk plasma frequency and τ the relaxation time of the conduction-band electrons of the metal. We neglect damping for now by putting $\tau^{-1} = 0$ in equation (8). The eigenmodes of the EM field, i.e., solutions of equation (3) in the absence of an incident field, are obtained at the poles of $T_{P\ell}$. It can be shown from equations (4) and (5) that, below ω_p, such poles exist near the real frequency axis only for $P = E$. These poles are in the lower complex frequency half plane at $z_\ell = \tilde{\omega}_\ell - \mathrm{i}\Gamma_\ell$; $\tilde{\omega}_\ell$ is the eigenfrequency while Γ_ℓ denotes the inverse of the lifetime of the respective mode. For $qS \ll 1$, the eigenfrequencies of these so-called surface– or particle–plasmon (because they correspond to 2^ℓ-pole collective electron oscillations at the surface of the particle) modes are given by $\tilde{\omega}_\ell \simeq \omega_p\sqrt{\ell/[\ell + (\ell + 1)\epsilon]}$, $\ell = 1, 2, \ldots$, while $\Gamma_\ell/\tilde{\omega}_\ell \ll 1$. The density of states of the particle–plasmon modes can be deduced directly from equation (6): if the function $(1 + T_{E\ell})(1 + T_{H\ell})$ is analytic in the complex frequency plane except at $z_\ell = \tilde{\omega}_\ell - \mathrm{i}\Gamma_\ell$ where it has a simple pole due to the pole of $T_{E\ell}$, making a Laurent expansion in the vicinity of z_ℓ on the real axis (we remember that $\Gamma_\ell/\tilde{\omega}_\ell \ll 1$), and keeping the leading term $\alpha_\ell/(\omega - z_\ell)$, we obtain

$$\begin{aligned} \Delta N_\ell(\omega) &\simeq \frac{2\ell + 1}{\pi} \operatorname{Im} \ln \alpha_\ell - \frac{2\ell + 1}{\pi} \arctan \frac{\Gamma_\ell}{\omega - \tilde{\omega}_\ell} \\ &\Rightarrow \Delta n_\ell(\omega) \simeq \frac{2\ell + 1}{\pi} \frac{\Gamma_\ell}{(\omega - \tilde{\omega}_\ell)^2 + \Gamma_\ell^2}, \end{aligned} \tag{9}$$

i.e., the change of the partial density of states, $\Delta n_\ell(\omega)$, is a Lorentzian centred at $\tilde{\omega}_\ell$ with a half width at half maximum equal to Γ_ℓ. Since $\Gamma_\ell/\tilde{\omega}_\ell \ll 1$, these particle–plasmon modes resemble bound states: they have a long (though not infinite) lifetime and the field intensity associated with them is mostly concentrated at the particle (though it leaks, to some minor degree, in the host region). Such states are referred to as *virtual bound states*.

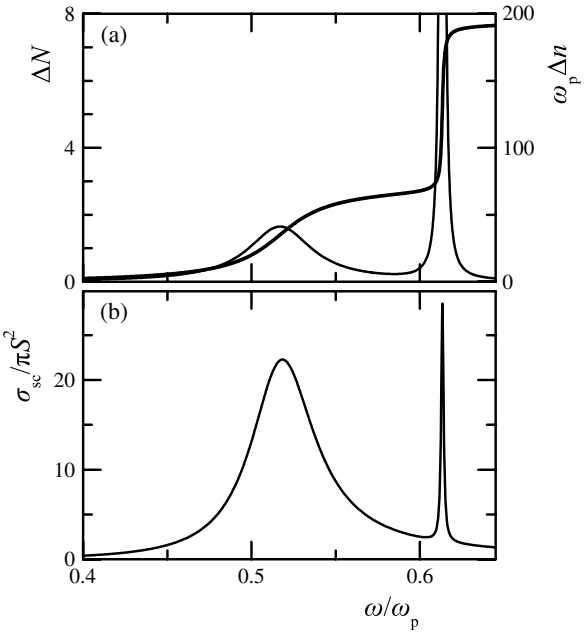

Figure 1. (a) The change in the number of states ΔN (thick curve) and in the density of states Δn (thin curve) induced by a non-absorbing metallic sphere of radius $S = c/\omega_p$, in air. (b) The corresponding scattering cross section.

In figure 1(a) we show the change in the number and in the density of states induced by a non-absorbing metallic sphere in air, in the frequency region of the first two particle–plasmon modes. The sphere has a radius $S = c/\omega_p$, which for $\hbar\omega_p = 10$ eV corresponds to about 20 nm. It can be seen that Δn is characterized by two resonance peaks and is nicely fitted by two Lorentzian curves given by equation (9): the first with $\ell = 1$, $\tilde{\omega}_1 = 0.517\omega_p$, $\Gamma_1 = 0.0232\omega_p$, and the second with $\ell = 2$, $\tilde{\omega}_2 = 0.613\omega_p$, $\Gamma_2 = 0.0009\omega_p$. The values of z_1 and z_2 obtained in this way define with a relative error of the order of 0.0001 the poles of T_{E1} and T_{E2}, respectively. It can be directly deduced from equation (7) that the scattering cross section also exhibits resonance peaks at $\tilde{\omega}_1$ and $\tilde{\omega}_2$, which are indeed observed in figure 1(b).

3. A periodic monolayer of metallic nanospheres

We now consider a plane of non-overlapping spheres at $z = 0$: an array of spheres centred on the sites of a 2D lattice specified by $\mathbf{R}_n = n_1\mathbf{a}_1 + n_2\mathbf{a}_2$, where $\mathbf{a}_1$ and $\mathbf{a}_2$ are primitive vectors in the xy plane and $n_1, n_2 = 0, \pm1, \pm2, \pm3, \ldots$. The corresponding 2D reciprocal lattice is obtained in the usual manner as follows: $\mathbf{g} = m_1\mathbf{b}_1 + m_2\mathbf{b}_2$, with $m_1, m_2 = 0, \pm1, \pm2, \pm3, \ldots$ and $\mathbf{b}_1, \mathbf{b}_2$ defined by $\mathbf{b}_i \cdot \mathbf{a}_j = 2\pi\delta_{ij}$, where $i, j = 1, 2$.

We assume that a plane EM wave of wavevector $\mathbf{q}$ is incident on the plane of spheres from the left ($z < 0$). Due to the 2D periodicity of the structure under consideration, the component of the wavevector parallel to the plane of spheres, $\mathbf{q}_\parallel$, can always be written as $\mathbf{q}_\parallel = \mathbf{k}_\parallel + \mathbf{g}'$, where the reduced wavevector $\mathbf{k}_\parallel$ lies in the surface Brillouin zone (SBZ) and $\mathbf{g}'$ is an appropriate reciprocal vector of the given lattice. Writing $\mathbf{q} = \mathbf{k}_\parallel + \mathbf{g}' + \left[q^2 - (\mathbf{k}_\parallel + \mathbf{g}')^2\right]^{1/2}\hat{\mathbf{e}}_z \equiv \mathbf{K}^+_{\mathbf{g}'}$, where $\hat{\mathbf{e}}_z$ is the unit vector along the z axis, the electric-field component $\mathbf{E}_{\rm in}(\mathbf{r})$ corresponding to the incident plane EM wave, expressed with respect to an origin $\mathbf{A}_l$ on the left of the plane

of spheres, has the form

$$\mathbf{E}_{\rm in}(\mathbf{r}) = [E_{\rm in}]^{+}_{\mathbf{g}'i'} \exp\left[\mathrm{i}\mathbf{K}^{+}_{\mathbf{g}'} \cdot (\mathbf{r} - \mathbf{A}_{\rm l})\right] \hat{\mathbf{e}}_{i'}, \tag{10}$$

where $i' = 1$ or 2 specifies the polarization mode: $\hat{\mathbf{e}}_1$ and $\hat{\mathbf{e}}_2$ are the polar and azimuthal unit vectors, respectively, which are perpendicular to $\mathbf{K}^{+}_{\mathbf{g}'}$.

Since ω and $\mathbf{k}_\parallel$ are conserved quantities in the scattering process, the field scattered by the plane of spheres will consist of a series of plane waves with wavevectors

$$\mathbf{K}^{\pm}_{\mathbf{g}} = \mathbf{k}_\parallel + \mathbf{g} \pm \left[q^2 - (\mathbf{k}_\parallel + \mathbf{g})^2\right]^{1/2} \hat{\mathbf{e}}_z, \qquad \forall \mathbf{g} \tag{11}$$

and polarizations along $\hat{\mathbf{e}}_1$ and $\hat{\mathbf{e}}_2$ (polar and azimuthal unit vectors, respectively, associated with every $\mathbf{K}^{s}_{\mathbf{g}}$, $s = \pm$). We note that when $(\mathbf{k}_\parallel + \mathbf{g})^2 > q^2$ the corresponding wave decays to the right for $s = +$, and to the left for $s = -$; and the corresponding unit vectors $\hat{\mathbf{e}}_i$ become complex. The transmitted wave (incident + scattered), expressed with respect to an origin $\mathbf{A}_{\rm r}$ on the right of the plane of spheres, has the form

$$\mathbf{E}^{+}_{\rm tr}(\mathbf{r}) = \sum_{\mathbf{g}i} [E_{\rm tr}]^{+}_{\mathbf{g}i} \exp\left[\mathrm{i}\mathbf{K}^{+}_{\mathbf{g}} \cdot (\mathbf{r} - \mathbf{A}_{\rm r})\right] \hat{\mathbf{e}}_i, \qquad z > 0, \tag{12}$$

with

$$[E_{\rm tr}]^{+}_{\mathbf{g}i} = [E_{\rm in}]^{+}_{\mathbf{g}'i'} \delta_{\mathbf{g}\mathbf{g}'}\delta_{ii'} + [E_{\rm sc}]^{+}_{\mathbf{g}i} = Q^{\rm I}_{\mathbf{g}i;\mathbf{g}'i'} [E_{\rm in}]^{+}_{\mathbf{g}'i'} \tag{13}$$

and the reflected wave, expressed with respect to $\mathbf{A}_{\rm l}$, has the form

$$\mathbf{E}^{-}_{\rm rf}(\mathbf{r}) = \sum_{\mathbf{g}i} [E_{\rm rf}]^{-}_{\mathbf{g}i} \exp\left[\mathrm{i}\mathbf{K}^{-}_{\mathbf{g}} \cdot (\mathbf{r} - \mathbf{A}_{\rm l})\right] \hat{\mathbf{e}}_i, \qquad z < 0, \tag{14}$$

with

$$[E_{\rm rf}]^{-}_{\mathbf{g}i} = [E_{\rm sc}]^{-}_{\mathbf{g}i} = Q^{\rm III}_{\mathbf{g}i;\mathbf{g}'i'} [E_{\rm in}]^{+}_{\mathbf{g}'i'}\,. \tag{15}$$

The above equations define the elements of the transmission ($Q^{\rm I}$) and reflection ($Q^{\rm III}$) matrices for a plane wave incident on the plane of spheres from the left. They depend on the scattering properties of the individual scatterer, on the geometry of the plane, and of course on the frequency, the angle of incidence, and the polarization of the incident wave. Similarly, we can define the transmission matrix elements, $Q^{\rm IV}_{\mathbf{g}i;\mathbf{g}'i'}$, and the reflection matrix elements, $Q^{\rm II}_{\mathbf{g}i;\mathbf{g}'i'}$, for a plane wave incident on the plane of spheres from the right. Explicit expressions for these Q matrices can be found elsewhere [10–12].

After calculating the transmitted and reflected waves on the right and left of the plane of spheres, when the plane wave of equation (10) is incident on it from the left, we can proceed to the calculation of the transmittance $\mathcal{T}(\omega, \mathbf{k}_\parallel + \mathbf{g}', i')$ and the reflectance $\mathcal{R}(\omega, \mathbf{k}_\parallel + \mathbf{g}', i')$ of the plane. These are defined as the ratio of the transmitted, respectively the reflected, energy flux to the energy flux associated with the incident wave. We obtain

$$\mathcal{T} = \frac{\sum_{\mathbf{g}i} |[E_{\rm tr}]^{+}_{\mathbf{g}i}|^2 K^{+}_{\mathbf{g}z}}{|[E_{\rm in}]^{+}_{\mathbf{g}'i'}|^2 K^{+}_{\mathbf{g}'z}} \tag{16}$$

and

$$\mathcal{R} = \frac{\sum_{\mathbf{g}i} |[E_{\rm rf}]^{-}_{\mathbf{g}i}|^2 K^{+}_{\mathbf{g}z}}{|[E_{\rm in}]^{+}_{\mathbf{g}'i'}|^2 K^{+}_{\mathbf{g}'z}}. \tag{17}$$

We remember that only propagating beams (those with $K^{+}_{\mathbf{g}z}$ real) enter the numerators of the above equations. Finally, we note that if absorption is present it can be calculated from the requirement of energy conservation: $\mathcal{A} = 1 - \mathcal{T} - \mathcal{R}$.

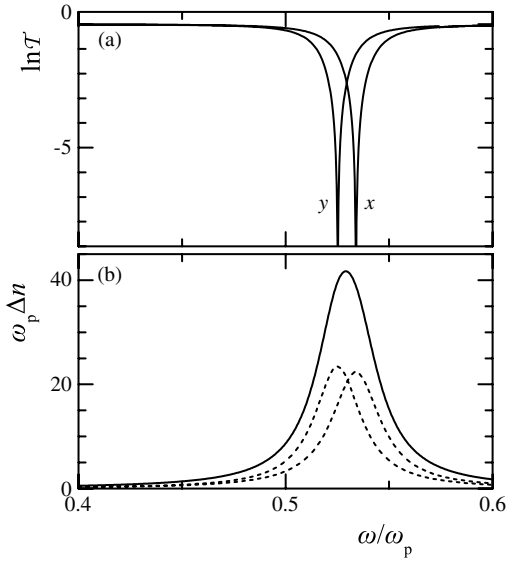

Figure 2. A rectangular array ($a_x = 8.5c/\omega_p$, $a_y = 6.8c/\omega_p$) of non-absorbing metallic spheres of radius $S = c/\omega_p$, in air. (a) Transmittance at normal incidence and polarization along x and y. (b) Change of the density of states of the system with respect to air, for $\mathbf{k}_\parallel = \mathbf{0}$. Δn is analysed in the two Lorentzian curves of unit area shown by the dashed curves.

The difference in the number of states up to a given frequency ω between the system under consideration (a plane of spheres in a homogeneous medium) and that of the homogeneous medium extending over all space is given by [14, 16]

$$\Delta N(\omega) = \frac{N}{A} \int \int_{\mathrm{SBZ}} \mathrm{d}^2 k_\parallel \Delta N(\omega, \mathbf{k}_\parallel), \tag{18}$$

where N is the number of surface unit cells of the plane of spheres, A is the area of the SBZ, and

$$\Delta N(\omega, \mathbf{k}_\parallel) = \frac{1}{2\pi} \operatorname{Im} \ln \det \mathbf{S}, \tag{19}$$

with the elements of the S matrix in the representation $\{s\mathbf{g}i\}$ given by

$$\begin{aligned}
S^{++}_{\mathbf{g}i;\mathbf{g}'i'} &= \exp\left[\mathrm{i}\left(\mathbf{K}^+_{\mathbf{g}'} \cdot \mathbf{A}_\mathrm{l} - \mathbf{K}^+_{\mathbf{g}} \cdot \mathbf{A}_\mathrm{r}\right)\right] Q^{\mathrm{I}}_{\mathbf{g}i;\mathbf{g}'i'} \\
S^{+-}_{\mathbf{g}i;\mathbf{g}'i'} &= \exp\left[\mathrm{i}\left(\mathbf{K}^-_{\mathbf{g}'} \cdot \mathbf{A}_\mathrm{r} - \mathbf{K}^+_{\mathbf{g}} \cdot \mathbf{A}_\mathrm{r}\right)\right] Q^{\mathrm{II}}_{\mathbf{g}i;\mathbf{g}'i'} \\
S^{-+}_{\mathbf{g}i;\mathbf{g}'i'} &= \exp\left[\mathrm{i}\left(\mathbf{K}^+_{\mathbf{g}'} \cdot \mathbf{A}_\mathrm{l} - \mathbf{K}^-_{\mathbf{g}} \cdot \mathbf{A}_\mathrm{l}\right)\right] Q^{\mathrm{III}}_{\mathbf{g}i;\mathbf{g}'i'} \\
S^{--}_{\mathbf{g}i;\mathbf{g}'i'} &= \exp\left[\mathrm{i}\left(\mathbf{K}^-_{\mathbf{g}'} \cdot \mathbf{A}_\mathrm{r} - \mathbf{K}^-_{\mathbf{g}} \cdot \mathbf{A}_\mathrm{l}\right)\right] Q^{\mathrm{IV}}_{\mathbf{g}i;\mathbf{g}'i'}
\end{aligned} \tag{20}$$

for the given ω and $\mathbf{k}_\parallel$. The phase factors in equation (20) arise from the need to refer all waves to a common origin.

We consider a rectangular array [$\mathbf{a}_1 = (a_x, 0)$ and $\mathbf{a}_2 = (0, a_y)$], with lattice constants $a_x = 8.5c/\omega_\mathrm{p}$ and $a_y = 6.8c/\omega_\mathrm{p}$, of non-absorbing metallic spheres with $S = c/\omega_\mathrm{p}$, in air. Figure 2(a) shows the transmittance of the plane of spheres at normal incidence. In the frequency region about the dipole surface–plasmon resonance of the individual spheres, there are two dips in the transmission spectrum. The first dip corresponds to plasma oscillations at the surface of the spheres parallel to the y axis and is excited when the incident field is polarized along the y axis. The second dip corresponds to surface-plasma oscillations parallel

to the x axis and is excited by x-polarized incident field. We see that the threefold degeneracy of the dipole surface–plasmon mode of the single sphere (the dipole plasma oscillations along x, y, z are in this case equivalent) has been removed because of the interaction with the other spheres of the plane. The dipole mode of the plane of spheres which corresponds to surface-plasma oscillations along the z axis, obviously, cannot be excited at normal incidence because of the transverse nature of the EM field; this dipole mode is a bound state of the system. The above analysis is consistent with our results for $\Delta n(\omega, \mathbf{k}_\parallel = \mathbf{0}) \equiv \partial \Delta N(\omega, \mathbf{k}_\parallel = \mathbf{0})/\partial\omega$ for the system under consideration. As can be seen in figure 2(b), we obtain two virtual bound states which are manifested in the density of states as Lorentzian curves centred at $0.525\omega_\mathrm{p}$ and $0.534\omega_\mathrm{p}$, in excellent agreement with the position of the dips in the corresponding transmission spectra. These two Lorentzian curves are obtained from a fit of the function $\Delta n(\omega, \mathbf{k}_\parallel = \mathbf{0})$ and reproduce perfectly the initial function. The integral of each Lorentzian equals unity, while its centre and half width at half maximum determine the eigenfrequency and inverse lifetime, respectively, of the corresponding virtual bound state. In addition, there is a bound state (a delta function in $\Delta n(\omega, \mathbf{k}_\parallel = \mathbf{0})$ which is not shown the figure; we find this by a direct numerical determination of the corresponding eigenfrequency) at $0.525\omega_\mathrm{p}$. At off-normal incidence all the dipole surface–plasmon modes can be excited, and are virtual bound states of the system. Indeed, in this case, a p-polarized incident wave has an electric-field component normal to the plane of spheres and can excite surface-plasma oscillations along the z axis as well. In general, in the case of a 2D lattice of metallic spheres, the dipole surface–plasmon virtual bound states of the individual spheres interact weakly between them and form three relatively narrow bands, $\omega(\mathbf{k}_\parallel)$, about the corresponding eigenfrequency of the single sphere. In the same manner, bands from higher 2^ℓ-pole surface–plasmon modes of the Drude spheres are formed at higher frequencies, but these will not concern us in the remaining of the paper; it has been established that resonance structures associated with such higher multipole modes are smoothed out if the actual dielectric function of the (simple) metal is employed [17].

4. A waveguide with a periodic monolayer of metallic nanospheres on it

One can use the same notation as that introduced in the previous section (the calculation is of course much easier) to describe the scattering properties of a homogeneous plate. In this case the Q matrices are diagonal in $\mathbf{g}$ because of the translation invariance parallel to the xy plane. Explicit expressions for these matrices are summarized elsewhere [11, 12].

A homogeneous dielectric plate, sandwiched between two semi-infinite media with refractive indices smaller than that of the plate, also supports, besides the scattering states, waveguide modes. Along any direction parallel to the plate these modes have the form of propagating waves with a wavevector $\mathbf{q}_\parallel$; along the normal direction they decay exponentially to zero away from the plate on either side of it. Following a standard analysis [18], it can be shown that there are transverse electric (TE) guided modes (the electric field oscillates parallel to the interfaces) and transverse magnetic (TM) guided modes (the magnetic field oscillates parallel to the interfaces). The dispersion curves of the guided modes for an indium tin oxide (ITO) film ($\epsilon_\mathrm{ITO} = 3.6$, $\mu_\mathrm{ITO} = 1$) in air are shown in figure 3(a). It can be seen that these modes lie outside the light cone in air and, therefore, cannot be excited by an externally incident wave. They cannot match continuously a propagating mode of the EM field outside the film; momentum and energy cannot be conserved simultaneously. When we put a 2D periodic array of particles on the film, waveguide modes can be transformed from bound to radiative through an umklapp process: a plane wave of wavenumber q, incident on the periodic array, generates a number of diffracted beams with wavevectors given by equation (11). If $q < |\mathbf{k}_\parallel + \mathbf{g}|$ we obtain evanescent diffracted beams which can match continuously the corresponding guided waves of

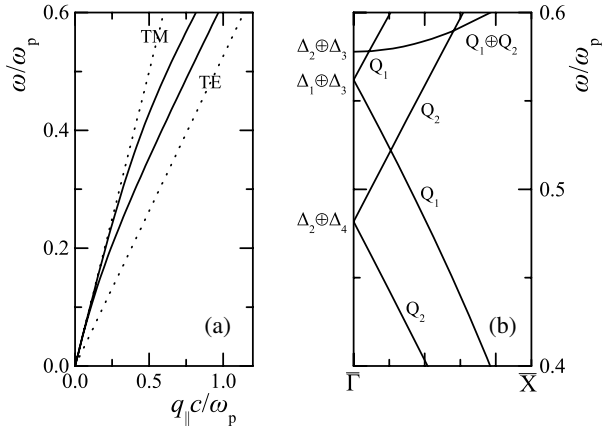

Figure 3. (a) Dispersion curves of the TE and TM waveguide modes for an ITO film, of thickness $d = 3c/\omega_p$, in air. The straight lines $\omega = cq_\parallel$ and $\omega = cq_\parallel/\sqrt{\epsilon_{ITO}}$ (shown by dotted lines) define the light cone in air and ITO, respectively. (b) The above dispersion curves in the frequency region from $0.4\omega_p$ to $0.6\omega_p$, folded within the SBZ of an (empty) rectangular lattice ($a_x = 8.5c/\omega_p$, $a_y = 6.8c/\omega_p$), along the $\overline{\Gamma X}$ direction. All these curves are now inside the light cone in air. The different bands are labelled by the appropriate irreducible representation of the point group of the wavevector (the C_{1h} group for the $\overline{\Gamma X}$ direction and the C_{2v} group for the $\overline{\Gamma}$ point).

the same polarization and of the same $\mathbf{q}_\parallel = \mathbf{k}_\parallel + \mathbf{g}$, provided that they have the right frequency. Accordingly, the waveguide modes are no longer bound within the film, but leak into the outer region becoming virtual bound states. These modes can be excited by an externally incident wave and manifest themselves as resonances in the transmission spectrum. From another point of view, because of the 2D periodicity of the coating layer, the waveguide frequency bands are folded within the SBZ of the given lattice and acquire a small imaginary part due to the mixing with the extended (scattering) states. Moreover, strong interaction, leading to level repulsion, will occur between all the virtual bound states of the system if they are close to each other in the complex frequency plane, provided that they have the same symmetry.

To demonstrate the folding of the dispersion curves of figure 3(a), we assume a lattice without scatterers on the waveguide (a so-called empty lattice). The resulting band structure in the reduced-zone scheme for a rectangular lattice is shown in figure 3(b). The waveguide modes which now appear within the light cone in air will, in principle, become virtual bound states when actual scatterers will occupy the lattice sites; the modes outside the light cone will remain bound. Along the symmetry lines of the SBZ, the waveguide modes have the symmetry of the irreducible representations of the point symmetry group of the corresponding wavevector [19], as shown in figure 3(b). Coupling between waveguide and continuum states is, of course, possible only if the symmetry of the folded bands is the same with that of an appropriate externally incident wave. For example, the electric-field associated with a normally incident plane EM wave has Δ_3 or Δ_4 symmetry if it is polarized along x or y, respectively. Therefore, at the $\overline{\Gamma}$ point, $\mathbf{k}_\parallel = (0, 0)$, the states which have Δ_1 and Δ_2 symmetry (see figure 3(b)) will remain bound, whereas those of Δ_3 and Δ_4 symmetry will become virtual bound states. Similarly, along the $\overline{\Gamma X}$ direction, $\mathbf{k}_\parallel = (k_x, 0)$, $0 < k_x < \pi/a_x$, the Q_2 and Q_1 bands inside the light cone in air will be excited by s- and p-polarized incident wave, respectively.

We shall now demonstrate the above on a specific example which corresponds to systems of other nanoparticles (ellipsoids and discs) studied experimentally [3, 6]: a rectangular array

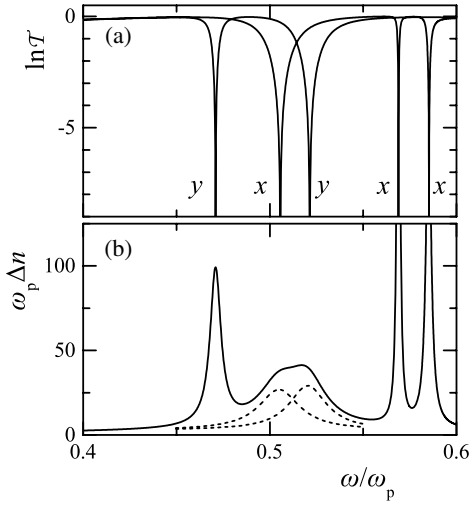

Figure 4. A rectangular array ($a_x = 8.5c/\omega_p$, $a_y = 6.8c/\omega_p$) of non-absorbing metallic spheres of radius $S = c/\omega_p$ on top of an ITO film of thickness $d = 3c/\omega_p$, in air. (a) Transmittance at normal incidence and polarization along x and y. (b) Change of the density of states of the system with respect to air, for $\mathbf{k}_\parallel = \mathbf{0}$. Δn consists essentially of five Lorentzian curves of unit area (by the dashed curves we show the analysis of a double Lorentzian).

($a_x = 8.5c/\omega_p$, $a_y = 6.8c/\omega_p$) of metallic spheres, of radius $S = c/\omega_p$, on top of an ITO film, of thickness $d = 3c/\omega_p$. The transmission and reflection matrices for the composite slab, to be denoted by $\mathbf{Q}$, are obtained by combining the matrices $\mathbf{Q}(1)$ and $\mathbf{Q}(2)$ of its constituents: the array of metallic spheres on the left (denoted by 1) and the ITO film on the right (denoted by 2), in air. Taking $\mathbf{A}_r(1)$, the origin on the right of the plane of spheres, the same point as $\mathbf{A}_l(2)$, the origin on the left of the waveguide in the air region, one can easily show that

$$\begin{aligned}
\mathbf{Q}^{\mathrm{I}} &= \mathbf{Q}^{\mathrm{I}}(2)\left[\mathbf{I} - \mathbf{Q}^{\mathrm{II}}(1)\mathbf{Q}^{\mathrm{III}}(2)\right]^{-1}\mathbf{Q}^{\mathrm{I}}(1) \\
\mathbf{Q}^{\mathrm{II}} &= \mathbf{Q}^{\mathrm{II}}(2) + \mathbf{Q}^{\mathrm{I}}(2)\mathbf{Q}^{\mathrm{II}}(1)\left[\mathbf{I} - \mathbf{Q}^{\mathrm{III}}(2)\mathbf{Q}^{\mathrm{II}}(1)\right]^{-1}\mathbf{Q}^{\mathrm{IV}}(2) \\
\mathbf{Q}^{\mathrm{III}} &= \mathbf{Q}^{\mathrm{III}}(1) + \mathbf{Q}^{\mathrm{IV}}(1)\mathbf{Q}^{\mathrm{III}}(2)\left[\mathbf{I} - \mathbf{Q}^{\mathrm{II}}(1)\mathbf{Q}^{\mathrm{III}}(2)\right]^{-1}\mathbf{Q}^{\mathrm{I}}(1) \\
\mathbf{Q}^{\mathrm{IV}} &= \mathbf{Q}^{\mathrm{IV}}(1)\left[\mathbf{I} - \mathbf{Q}^{\mathrm{III}}(2)\mathbf{Q}^{\mathrm{II}}(1)\right]^{-1}\mathbf{Q}^{\mathrm{IV}}(2).
\end{aligned} \tag{21}$$

All matrices refer of course to the same ω and $\mathbf{k}_\parallel$. Therefore, for a plane wave $[E_{\mathrm{in}}]^+_{\mathbf{g}'i'} \exp\{\mathrm{i}\mathbf{K}^+_{\mathbf{g}'} \cdot [\mathbf{r} - \mathbf{A}_l(1)]\}\hat{\mathbf{e}}_{i'}$, incident on the slab from the left, we finally obtain a reflected wave $\sum_{\mathbf{g}i} [E_{\mathrm{rf}}]^-_{\mathbf{g}i} \exp\{\mathrm{i}\mathbf{K}^-_{\mathbf{g}} \cdot [\mathbf{r} - \mathbf{A}_l(1)]\}\hat{\mathbf{e}}_i$ on the left of the slab and a transmitted wave $\sum_{\mathbf{g}i} [E_{\mathrm{tr}}]^+_{\mathbf{g}i} \exp\{\mathrm{i}\mathbf{K}^+_{\mathbf{g}} \cdot [\mathbf{r} - \mathbf{A}_r(2)]\}\hat{\mathbf{e}}_i$ on the right of the slab, where $\mathbf{A}_l(1)(\mathbf{A}_r(2))$ is the chosen origin on the left (right) of the slab, and $[E_{\mathrm{tr}}]^+_{\mathbf{g}i}$, $[E_{\mathrm{rf}}]^-_{\mathbf{g}i}$ are obtained with the help of the Q^{I}, Q^{III} matrices of the slab according to equations (13) and (15). The transmittance and reflectance of the slab are given by equations (16) and (17).

In figure 4(a) we show the transmittance of the composite system at normal incidence and polarization along x and y. The resonance structures at $0.505\omega_p$ and $0.520\omega_p$ arise from the excitation of the corresponding dipole particle–plasmon modes of the plane of spheres, of symmetry Δ_3 and Δ_4, respectively. It can be seen that these are shifted to lower frequencies (see also figure 2(a)), because of the presence of the waveguide. We note, again, that the mode which corresponds to dipole surface-plasma oscillations along the z axis cannot be excited at normal incidence; it is a bound state of the system (it has Δ_1 symmetry) at $0.475\omega_p$. In

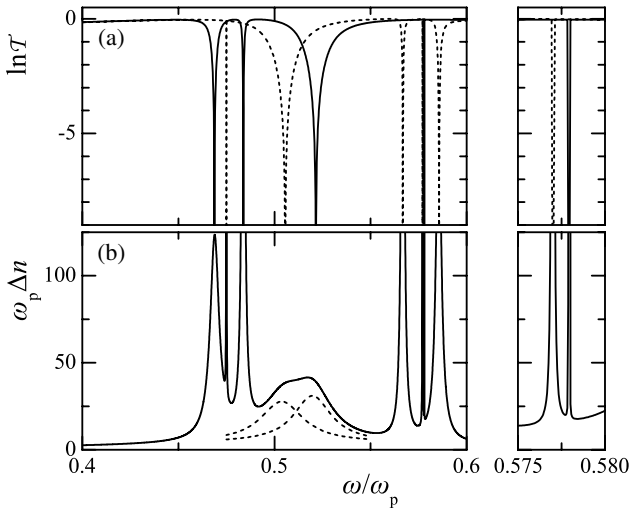

Figure 5. A rectangular array ($a_x = 8.5c/\omega_p$, $a_y = 6.8c/\omega_p$) of non-absorbing metallic spheres of radius $S = c/\omega_p$ on top of an ITO film of thickness $d = 3c/\omega_p$, in air. (a) Transmittance at off-normal incidence [$\mathbf{q}_\parallel = (0.03\pi/a_x, 0)$] and polarization s (solid curve) and p (dashed curve). (b) Change of the density of states of the system with respect to air, for $\mathbf{k}_\parallel = (0.03\pi/a_x, 0)$. Δn consists essentially of nine Lorentzian curves of unit area (by the dashed curves we show the analysis of a double Lorentzian). The resonance structures about $0.5775\omega_p$ are shown with a higher resolution in the margin.

addition, we observe in figure 4(a) three relatively sharp resonances which originate from appropriate waveguide modes (see figure 3(b)). The one at $0.471\omega_p$ corresponds to a TE mode and is excited by a y-polarized incident wave (it has Δ_4 symmetry). Correspondingly, that at $0.569\omega_p$ corresponds to a TM mode and is excited by an x-polarized incident wave (it has Δ_3 symmetry). Finally, that at $0.585\omega_p$ corresponds to a TE mode and is excited by an x-polarized incident wave (it has Δ_3 symmetry). The other three waveguide modes at the $\overline{\Gamma}$ point in the frequency region which interests us here, of Δ_1 and Δ_2 symmetry (see figure 3(b)), are not excited for symmetry reasons, as explained above, and remain bound. This analysis is consistent with our results for $\Delta n(\omega, \mathbf{k}_\parallel = \mathbf{0})$ for the system under consideration. We have nine distinct states: four bound states (delta functions in $\Delta n(\omega, \mathbf{k}_\parallel = \mathbf{0})$ which are not shown in figure 4(b); we find these by a direct numerical determination of the corresponding eigenfrequencies) at $0.475\omega_p$, $0.482\omega_p$, $0.575\omega_p$ and $0.578\omega_p$, and five virtual bound states which are manifested in the density of states as Lorentzian curves of unit area (see figure 4(b)) centred at $0.471\omega_p$, $0.505\omega_p$, $0.520\omega_p$, $0.569\omega_p$ and $0.585\omega_p$, in excellent agreement with the position of the resonance structures in the corresponding transmission spectra. The centre and half width at half maximum of each Lorentzian determine the eigenfrequency and inverse lifetime, respectively, of the corresponding virtual bound state.

At off-normal incidence all the above modes become virtually bound, and can be excited by an appropriate incident wave, as shown in figure 5. By varying $\mathbf{q}_\parallel$ along the $\overline{\Gamma X}$ direction, we deduce the corresponding dispersion curves of the virtual bound states of the system. The results are shown in figure 6, together with the dispersion curves of the waveguide modes of the ITO film and the surface–plasmon modes of the array of spheres in the absence of interaction with the waveguide modes (schematically shown by the horizontal lines), separately. It can be seen that states of the same symmetry interact and repel each other, giving rise to a band diagram of hybridized waveguide and particle–plasmon modes. It is worth noting that these

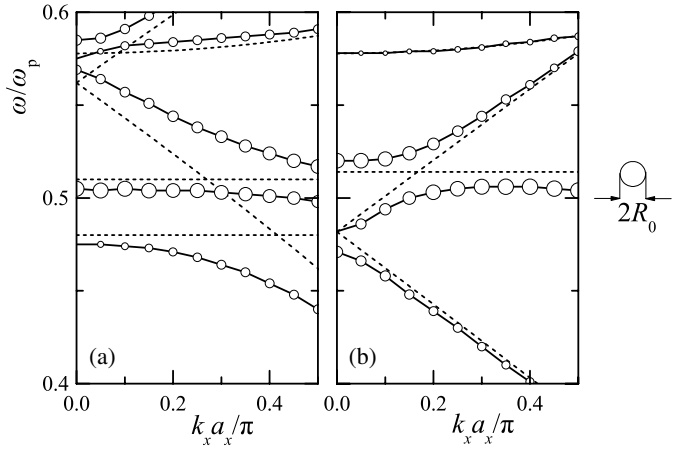

Figure 6. Dispersion curves of the virtual bound states of a rectangular array ($a_x = 8.5c/\omega_p$, $a_y = 6.8c/\omega_p$) of non-absorbing metallic spheres of radius $S = c/\omega_p$ on top of an ITO film of thickness $d = 3c/\omega_p$, in air, along the $\overline{\Gamma X}$ direction: $\mathbf{k}_\parallel = (k_x, 0)$ ((a): bands of Q_1 symmetry, (b): bands of Q_2 symmetry). The radius R of the circles about selected points gives the lifetime of the corresponding state: $\Gamma/\omega_p = 10^{-R_0/R}$, where R_0 is the radius of the circle in the margin. The dotted lines show the corresponding dispersion curves of the waveguide modes of the ITO film and the surface–plasmon modes of the array of spheres in the absence of interaction with the waveguide modes (schematically drawn by horizontal lines), separately.

modes are, in general, virtual bound states and not true bound states of the system. In other words, they have a long but finite lifetime, which corresponds to an imaginary part of the eigenfrequency typically a few orders of magnitude smaller than the real part, as shown in figure 6.

A quantitative comparison of our results with experimental ones is not possible, at this stage, because there are no experimental data available for spherical particles. However, our results explain qualitatively the experimental findings relating to similar systems of nanoellipsoids and nanodiscs. They reproduce the main features of the observed extinction spectra and the relatively large Rabi splitting in the interaction between waveguide and particle–plasmon modes [3, 6]. We note that the layer-multiple-scattering method can be extended to systems of non-spherical particles: the scattering properties of the individual particle enter only through the corresponding T matrix, and efficient methods for its numerical evaluation for non-spherical particles are available in the literature [20]. We are presently involved in some work along this direction. Finally, for a quantitative comparison with an actual experiment, dissipative losses (absorption) in the constituent materials must be taken into account. These losses for metals are at least of the same order of magnitude as the radiative losses; these can be easily included in calculations by the layer-multiple-scattering method (as stated in the introduction) and will result in a broadening of the corresponding peaks of the extinction spectra [21].

Acknowledgments

This work was supported by the Empeirikeion Foundation and by the research program "Kapodistrias" of the University of Athens. G Gantzounis is supported by the State Scholarships Foundation (I.K.Y.), Greece.

References

[1] Lamprecht B, Schider G, Lechner R T, Ditlbacher H, Krenn J R, Leitner A and Aussenegg F R 2000 *Phys. Rev. Lett.* **84** 4721

[2] Félidj N, Aubard J, Lévi G, Krenn J R, Schider G, Leitner A and Aussenegg F R 2002 *Phys. Rev.* B **66** 245407

[3] Linden S, Kuhl J and Giessen H 2001 *Phys. Rev. Lett.* **86** 4688

[4] Taleb A, Russier V, Courty A and Pileni M P 1999 *Phys. Rev.* B **59** 13350

[5] Pinna N, Maillard M, Courty A, Russier V and Pileni M P 2002 *Phys. Rev.* B **66** 045415

[6] Christ A, Linden S, Zentgraf T, Nau D, Tikhodeev S G, Gippius N A, Kuhl J, Schindler F, Holleitner A W, Stehr J, Crewett J, Lupton J, Klar T, Scherf U, Feldmann J, Dahmen C, von Plessen G and Giessen H 2004 *Photonic Crystals: Advances in Design, Fabrication, and Characterization* ed K Busch, S Lölkes, R B Wehrspohn and H Föll (New York: Wiley) p 85

[7] Christ A, Tikhodeev S G, Gippius N A, Kuhl J and Giessen H 2003 *Phys. Rev. Lett.* **91** 183901

[8] Christ A, Zentgraf T, Kuhl J, Tikhodeev S G, Gippius N A and Giessen H 2004 *Phys. Rev.* B **70** 125113

[9] Tikhodeev S G, Yablonskii A L, Muljarov E A, Gippius N A and Ishihara T 2002 *Phys. Rev.* B **66** 045102

[10] Stefanou N, Karathanos V and Modinos A 1992 *J. Phys.: Condens. Matter* **4** 7389

[11] Stefanou N, Yannopapas V and Modinos A 1998 *Comput. Phys. Commun.* **113** 49

[12] Stefanou N, Yannopapas V and Modinos A 2000 *Comput. Phys. Commun.* **132** 189

[13] Ohtaka K and Inoue M 1982 *Phys. Rev.* B **25** 677

[14] Sainidou R, Stefanou N and Modinos A 2004 *Phys. Rev.* B **69** 064301

[15] Ashcroft N W and Mermin N D 1976 *Solid State Physics* (New York: Saunders)

[16] Ohtaka K, Inoue J and Yamaguti S 2004 *Phys. Rev.* B **70** 035109

[17] Stefanou N and Modinos A 1991 *J. Phys.: Condens. Matter* **3** 8135

[18] Yariv A and Yeh P 2003 *Optical Waves in Crystals: Propagation and Control of Laser Radiation* (New York: Wiley)

[19] Cornwell J F 1969 *Group Theory and Electronic Energy Bands in Solids* (Amsterdam: North-Holland)

[20] Mishchenko M I, Travis L D and Lacis A A 2002 *Scattering, Absorption, and Emission of Light by Small Particles* (Cambridge: Cambridge University Press)

[21] Yannopapas V and Stefanou N 2004 *Phys. Rev.* B **69** 012408